LANGMUIR

Article

8-anilino-1-naphthalenesulfonate/layered double hydroxide ultrathin films: small anion assembly and its potential application as fluorescent biosensor

Ping Zhang, Ling Li, Yun Zhao, Zeyun Tian, Yumei Qin, and Jun Lu

Langmuir, **Just Accepted Manuscript** • DOI: 10.1021/acs.langmuir.6b01980 • Publication Date (Web): 11 Aug 2016

ACS Publications

Langmuir is published by the American Chemical Society. 1155 Sixteenth Street N.W., Washington, DC 20036

8-anilino-1-naphthalenesulfonate/layered double hydroxide ultrathin films: small anion assembly and its potential application as fluorescent biosensor

*Ping Zhang, Ling Li, Yun Zhao, Zeyun Tian, Yumei Qin and Jun Lu**

State Key Laboratory of Chemical Resource Engineering, Beijing University of Chemical Technology, Beijing 100029, China.

KEYWORDS: ANS, LDH, small anion assembly, fluorescent biosensor, polar environment

ABSTRACT: The fluorescent dye 8-anilino-1-naphthalenesulfonate (ANS) is a widely used fluorescent probe molecule for biochemistry analysis. This article reported the fabrication of ANS/layered double hydroxide nanosheets $(ANS/LDH)_n$ ultrathin films (UTFs) via the layer-by-layer small anion assembly technique based on electrostatic interaction and two possible weak interactions−hydrogen bond and induced electrostatic interaction between ANS and positive-charged LDH nanosheets. The obtained UTFs show long-range-ordered periodic layered stacking structure and weak fluorescence in dry air or water, but it split into three narrow strong peaks in weak polarity environment induced by the 2D confinement effect of the LDH laminate, the fluorescence intensity increases with decreasing of the solvent polarity, concomitant with blue shift of the emission peaks, which show good sensoring reversibility. Meanwhile, the UTFs

exhibit selective fluorescence enhancement to the BSA-like protein biomolecules, and the rate of fluorescence enhancement with the protein concentration is significantly different with the different protein aggregate state. The $(ANS/LDH)_n$ UTF has the potential to be a novel type of biological flourescence sensor materials.

Introduction

In recent years, the research of various biosensors to detect substances related with biological activities (such as nucleic molecules, proteins, metal ions, small molecules and enzymes) with high sensitivity and good binding linearity has aroused more and more interest. Among them, fluorescence biosensors exhibited high sensitivity, low background noises, efficiency, visualization, wide dynamic ranges and some other advantages, which was widely applied in the study of biological activities. Fluorescent biosensors are classically defined as biological or biomimetic components that bear a receptor moiety, responsible for recognition of a target or its biological activity, which is genetically, enzymatically or chemically coupled to one (or several) fluorescent probe(s), responsible for conversion of the recognition event into a detectable and measurable optical signals.[1] Now fluorescent biosensors have become pivotal for scientists to study biochemical pocesses. Since the 19th century, small molecule fluorescent probes have been used widely in biological sciences to label biomolecules, and to detect and monitor protein/protein interactions, conformational changes and enzymatic dynamics.[2] With the advances of various synthetic fluorescent probes by chemists, the development of nongenetic biosensors has been further extended, being a powerful alternative for biomolecular process study.[3]

The solvatochromic fluorescent dye 8-anilino-1-naphthalenesulfonate (ANS) has been widely used as a biological probe due to its varied fluorescence emission wavelength, quantum yield and lifetime, for the purpose of indicating the hydrophobic/hydrophilic environments,[4,5] interactive locations[6,7] and the different conformation of proteins.[8] Generally, the fluorescent properties of ANS changed as the variation of its microenvironment, conformation and specific solute–solvent interactions. Kosower and co-workers[9] had thoroughly studied the photophysical behavior of ANS in various solvents. There are two fluorescent states of ANS which differ in response to solvent polarity change. The light absorption of ANS leads to its excitation from ground state $S_{0,np}$ (nonplanar (NP) geometry) to a local excited state $S_{1,\,np}$ in weak polar solvents, which then experiences transition concomitant with intramolecular electron transfer to the more stable charge transfer (CT) state $S_{l,ct}$ in high polar solvents, and in polar medium the CT state decays and returns to the ground state $S_{0,np}$ via another intramolecular electron transfer concomitant with a weak green fluorescence and quenched blue fluorescence. And the $S_{1,\,np}$ state decays to the $S_{0,np}$ state accompanied an intense blue fluorescence in weak polar solvents,[10] mostly due to the restricted rotational motion of the phenylamino group of ANS in hydrophobic environment. Scheme 1 shows the molecular structure and the photoexcitation conversions process of ANS. In addition, the solid supramolecular environments, such as in solid complexeswith α-,β-,γ-cyclodextrin or cyclophane CP 66[11] and theintercalation of layered double hydroxide materials,[12,13] also can affect the peculiar fluorescence behavior of ANS.

The layer-by-layer (LbL) assembly technique has been well established as a simple and versatile method of constructing composite ultrathin films (UTFs) with controlled thickness through the sequential adsorption of host and guest molecules by molecular interactions (e.g., electrostatic interactions,[14,15] covalent bonding,[16,17] hydrogen bonding,[18,19] DNA

hybridization,[20,21] streptavidin−biotin binding,[22] and so on). Recent reviews highlight the fabrication of various multicharged dye ions and polyion multilayer films.[23-25] However, it is quite hardly to introduce less-charged small ions into a LbL assembled film because they can be extracted more easily than polyions. Therefore, it is very desirable to achieve a new approach to fabricating stable UTFs containing small ions without any polyions involved, which will combine the merits of the LbL technique and the intrinsic advantages of the organic small ions.

Among the solid inorganic matrices used to accommodate organic dye molecules, layered double hydroxides (LDHs) materials have attracted much interest.[25,26] The LDHs generally expressed as $[M^{II}_{1-x}M^{III}_{x}(OH)_2](A^{n-})_{x/n} \cdot mH_2O$ (where M^{II} and M^{III} are divalent and trivalent metals, respectively, and A^{n-} is the guest anions that are present between hydroxide layers), which is a kind of anionic layered solid solution materials, has been applied in various fields such as catalytic,[27] adsorption,[28] separating materials,[29] functional auxiliary materials,[30] biomedical materials[31] and so on. As a typical anionic inorganic layered material, LDHs laminates can be exfoliated into LDHs nanosheets,[32,33] which provides the basis for the construction of multifunctional composite thin film material. Based on the electrostatic interaction, our previous works have realized the assembly of functional polyanion with LDHs nanosheets,[34,35] and developed the co-assembly method to assemble the LDHs nanosheets with the small anion/cation and polyanion blends,[36,37] and even the neutral small molecules wrapped up by the block copolymer micelles.[38,39] Based on hydrogen bonding interaction/Van der Waal interaction, the assembly of neutral polymer (with $-NH_2$ and –OH) with LDHs nanosheets have been realized,[40] and the co-assembly of the LDHs nanosheets with neutral small molecules/neutral metal complexes and neutral polymer blends were developed.[41,42] At the same

time, the assembly of some complex biological molecules (such as proteins, nucleic acids) with LDHs nanosheets was also realized.[43,44]

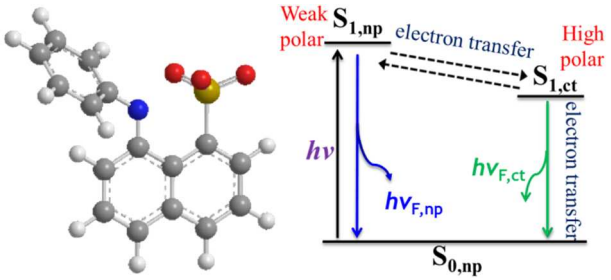

Scheme 1. The molecular structure (C grey, H white, O red, N blue, S yellow) and the photoexcitation conversions process of ANS. The phenylamino group is noncoplanar against the naphthalene ring as shown. The symbols used are: $h\nu$, excitation energy; $h\nu_{F,np}$, fluorescence emission from the $S_{1,np}$ state; $h\nu_{F,ct}$, fluorescence emission from the $S_{1,ct}$ state.

In previous work, Sun[13] reported ANS and a series of surfactants were cointercalated into the galleries of ZnAl-LDH by the anion exchange method. The films exhibit enhanced photo/thermo stability. In addition, the composite films show fluorescence anisotropy, attributed to the preferential orientation of ANS in the LDH gallery. However, there is no report on $(ANS/LDH)_n$ UTFs. Herein, we demonstrates the successful fabrication of ordered $(ANS/LDH)_n$ UTFs only by small ion LbL assembly technique. The obtained $(ANS/LDH)_n$ UTFs show uniform and long-range-ordered periodic layered structure. Moreover, the composite UTFs exhibit reversible fluorescence response for different polarity environment and the original broad fluorescence peak split into three induced by the 2D confinement effect of the LDH monolayers and the change of the polar environment, which is different with the ANS-intercalated LDH powders. This UTFs also exhibit selective fluorescence response of protein biomolecules, which is potential to be a novel type of flourescence bisensor material.

Experimental Section

Materials: 8-Anilino-1-naphthalenesulfonic acid, pancrelipase and Tris(hydroxymethyl) aminomethane were purchased from Shanghai Aladdin Biochemical Technology Co., Ltd. Albumin from Bovine Serum, glucose and tyrosine were purchased from J&K Chemical. Co. Ltd. Concanavalin was purchased from Beijing InnoChem Science & Technology Co. Ltd. Analytical grade NaOH, $Mg(NO_3)_2 \cdot 6H_2O$, $Al(NO_3)_3 \cdot 9H_2O$, petroleum ether, toluene, ethyl acetate, dimethyl formamide, ethanol, $NH_3 \cdot H_2O$, H_2O_2, H_2SO_4, $MgCl_2$,$CaCl_2$, and NaCl were purchased from Beijing Chemical Co. Ltd. All these reagents were used without further purification. Deionized and decarbonated water was used throughout the experimental process. Ultrapure water was made by the milipore Ultrapure Water Purifier from RephiLe Bioscience, Co. Ltd.

Preparation of $(ANS/LDH)_n$ ultrathin films: A colloidal LDH suspension was prepared according to the separate nucleation and aging steps (SNAS) method reported previously.[45] 80 mL NaOH (0.18 mol) solution and 70mL salt solution (0.06 mol $Mg(NO_3)_2 \cdot 6H_2O$ and 0.03 mol $Al(NO_3)_3 \cdot 9H_2O$) were simultaneously added to a colloid mill and mixed for 1 min with a rotor speed of 3000rpm. The resulting slurry was removed and heated at 100℃ for 24 hours. The product was washed three times with deionized and decarbonated water every time, a stable homogeneous MgAl-LDH suspension with a narrow size distribution can be obtained when the product was washed after four times. The concentration of LDH colloidal particles used for the fabrication of the thin film materials was 0.10% (*wt*%). The quartz glass substrates were cleaned in a mixed solution of concentrated H_2SO_4/30% H_2O_2 (vol : vol = 7 : 3) for 30 min and then washed by anhydrous alcohol and deionized water thoroughly. The quartz substrate was immersed in the LDH colloidal suspension ($1g \cdot L^{-1}$) for 15 min followed by through washing with deionized water and drying in a nitrogen gas flow at room temperature, and then the

substrate was treated with ANS solution (100 mg·L^{-1}, Tris buffer solution pH=8) for 15 min, washed several times with deionized water and dried in a nitrogen gas flow for 2 min at room temperature. The $(ANS/LDH)_n$ UTFs were fabricated by alternatively deposition of LDH colloidal suspension and ANS solution for *n* cycles, and after every deposition, the ultrathin film was washed several times with deionized water and dried under a nitrogen gas flow for 2 min at room temperature.

Characterization: UV−vis absorption spectra were collected on a Shimadzu U-3600 spectrophotometer with the slit width of 1.0 nm.Fluorescence spectra were obtained on a FL-4600 fluorospectrophotometer with an identical condition for comparison. The polarized fluorescence spectra were recorded with an Edinburgh Instruments' FL 900 fluorimeter. Small-angle XRD pattern of the films were obtained with a Rigaku 2500VB2+ PC diffractometer using Cu Kα radiation (λ= 1.541844 Å, 2θ= 0.5 − 8°) at 40 kV, 50 mA, with the step-scanned mode with 0.04°(2θ) per step and count time of 10s per step. A scanning electron microscope (SEM Zeiss Supra 55) was used to investigate the morphology of LDH and films. Atomic force microscope (AFM) software (Digital Instruments, Version 6.12) was used to obtain the surface roughness data. The attenuated total reflectance-Fourier transform infrared (ATR-FTIR) spectra were obtained using a Vector 22 (Bruker) spectrophotometer with 2 cm^{-1} resolution.

Results and Discussion

1 Assembly of the $(ANS/LDH)_n$ UTFs

ANS ions were assembled with Mg_2Al-NO_3 LDH nanosheets to obtain the $(ANS/LDH)_n$ composite films by layer by layer method, which was similar to the ordinary electrostatic assembly of anions with LDHs nanosheets, except that the LDH nanosheets were prepared by

separate nucleation and aging steps (SNAS) method as reported previously,[45] and the XRD pattern and SEM image of the Mg_2Al-NO_3 LDH powders are shown in Figure S1. The multilayer assembly process of the $(ANS/LDH)_n$ (n = 4 − 20) UTFs deposited on quartz substrates was monitored by UV-visible absorption spectroscopy (Figure 1). The absorption bands at 220, 275, 409 nm of the $(ANS/LDH)_n$ UTFs can be attributed to that of ANS, which shows red shift compared with that of the pristine ANS solution (Figure S2), suggesting the aggregation of the ANS ions in the UTFs. Meanwhile, the absorption intensities at 220, 275, 409 nm correlate nearly linearly with the number of bilayers n, which suggests that a stepwise and regular deposition procedure with almost equal amounts of ANS and LDH incorporated in each cycle, and the LbL assembly process for $(ANS/LDHs)_n$ UTF was well-defined and can be repeated upto 40 cycles at least.

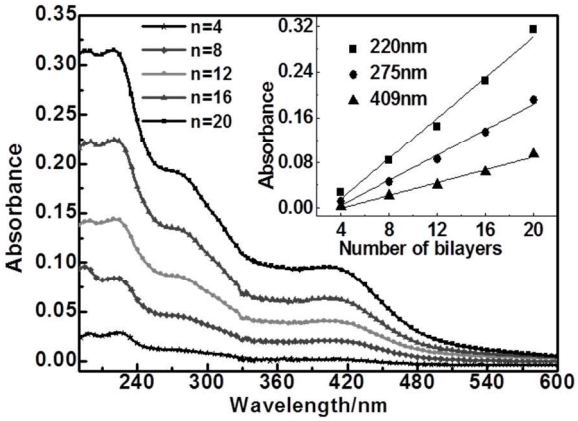

Figure 1. UV-Vis absorption spectra of $(ANS/LDH)_n$ (n = 4− 20) UTFs, inset: the plots of absorbance at 220, 275, 409 nm versus n.

In the normal case, due to polyanion have numerous negative charges which can be assembled easily with LDH nanosheets to form stable multilayer UTFs by electrostatic LbL assembly. But ordinary small anion is liable to fall off and hardly to assemble solely with LDH nanosheets

directly. Previous works showed that the small anions can be assembled with LDH nanosheets by blending with polyanion or incorporating in the block copolymer micelles.[36-39] It was found that the small anions only with multiple valent negative charges can be directly assembled with LDH nanosheets, such as zinc tetrasulfophthalocyanine $(ZnTSPc)^{4-}$,[46] trans-(1,10-phenanthroline-4,7-diphenyl sulfonate) ruthenium (Ⅱ) complex anion $[Ru(dpds)_3]^{4-}$,[47] and so on. In this work, the small anion ANS was assembled successfully with MgAl-LDH nanosheets to obtain the $(ANS/LDH)_n$ UTFs, in contrast to the traditional anion electrostatic assembly with the positive-charged LDH nanosheets. ANS has only one negatively charge at sulfonate group, but it has an imino group -NH- which may be formed hydrogen bond (O−H···N or N−H···O) network with the hydroxyl groups on the LDH monolayers. This hydrogen bond interaction can also facilitate the assembly of ANS with LDH nanosheets. The direct evidence for hydrogen bonding interaction within the UTF was obtained by attenuated total reflectance-Fourier transform infrared (ATR-FTIR) spectroscopy. The O–H stretching vibration of the LDH was used to estimate the strength of the hydrogen-bond interaction[41,42] between ANS and LDH, which leads to the characteristic peak intensity and position change in the IR absorption. The spectra of LDH-NO_3 and the $(ANS/LDH)_{50}$ UTF were compared (Supporting Information, Figure S7). It was found that the strong O–H vibration bands had a small shift down to 3400 cm^{-1} and became broad, compared with the bands at 3450 cm^{-1} for LDH-NO_3. Here, the O–H vibration bands had no very large shift but became broad, which was due to the formation of hydrogen-bond interaction between ANS and LDH nanosheets, but it still existed plentiful–OH which did not participate in the formation of hydrogen-bond interaction. These results supported that the hydrogen bonding interaction played an important role for this layer-by-layer assembly process.

Moreover, ANS has an unsaturated π conjugated electron, being highly delocalized, and it is possible that the induced electrostatic interaction occurred between the delocalized π electron system of ANS and the positive-charged LDH nanosheets. Overall, it has not only electrostatic interaction between the small anion ANS and positive LDH nanosheets, but also two kind of possible weak interactions in the $(ANS/LDH)_n$ system, hydrogen bond and induced electrostatic interaction, to facilitate the assembly of small anion and LDH nanosheets. Therefore, this result extended the LDHs-based LbL assembly method, that is the multiple interaction can be the driving force for small ions assembly for LDHs-based UTFs.

2 Morphology and structure characterization of the $(ANS/LDH)_n$ UTFs

The SEM and AFM were used to explore the surface morphology and thickness of the $(ANS/LDH)_n$ UTFs. Small-angle XRD measurement was used to check the periodic structure of the composite films. The alternative deposition of the LDH nanosheets and ANS by electrostatic interaction would lead to a periodic orderly UTFs stacked with the *ab*-plane ofLDH nanosheets lying on the substrate.

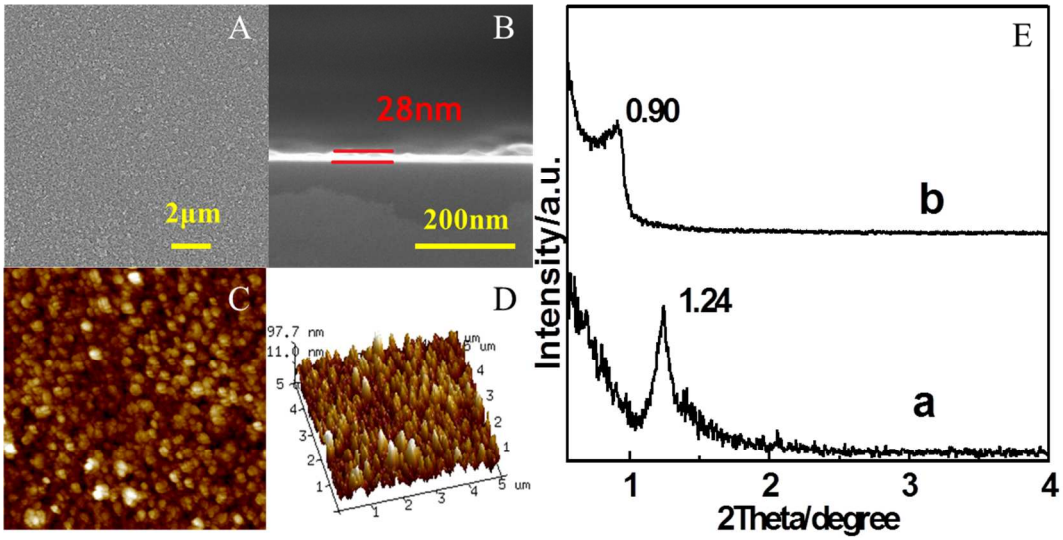

Figure 2. Morphology characterization of $(ANS/LDH)_4$ UTF: A) top-view SEM image, B) side-view SEM image, C) and D) tapping-mode AFM topographical image, scanning area is random for 5μm × 5μm; E) Small-angle XRD pattern for the $(ANS/LDH)_{40}$ UTFs in dry air (a) and after immersion treatment in petroleum ether (b).

The top view of SEM images (Figure 2A and S3) show that the film surface is microscopically continuous and smooth, and the side view of SEM images (Figure 2B and S3) show that the thickness of the $(ANS/LDH)_n$ (n = 4−20) UTFs approximately linearly increase upon increasing the bilayer number, and thus the average thickness can be estimated to be 7.2 nm per ANS/LDH bilayer cycle. The top view AFM images (5μm × 5μm) of $(ANS/LDH)_n$ (n = 4−20) (Figure 2C, D and S4) show that the film surface is uniform, and the root mean square roughness and average roughness of the UTFs are increased with the increasing bilayer number n (Table S1). Small-angle X-ray diffraction (XRD) pattern of $(ANS/LDH)_{40}$ UTF is shown in Figure 2E, which revealed that the UTF is significantly ordered along the normal with a strong Bragg peak at 1.24° (2θ) in dry air, corresponding to a spacing of about 7.0 nm, consistent with that of the side-view SEM results. This further confirmed that the $(ANS/LDH)_n$ UTFs present uniform and periodic layered structure, in agreement with the behaviors revealed by the absorption spectra mentioned above. These results implied that the LbL assembly based on electrostatic interaction and weak interactions between the samll anion and LDH nanosheets can hold the integrality of UTFs and the bilayer number n can be up to 40 at least.

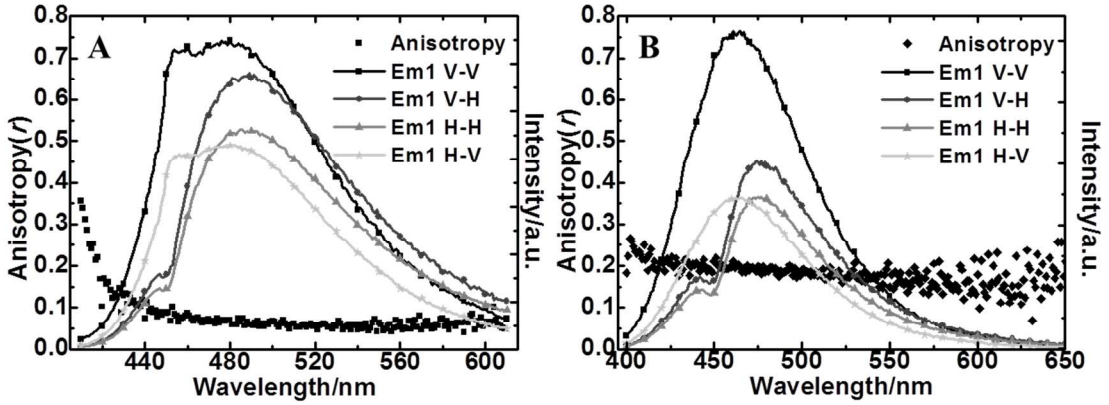

Figure 3. Polarized fluorescence profiles for the VV, VH, HH, HV modes and anisotropic value (*r*) for the A) ANS spin-coating thin film and B) $(ANS/LDH)_{20}$ UTF.

To investigate the microenvironment of the assembled ANS anions between the LDH nanosheets of the UTFs, the polarized luminescence spectra of the UTFs were measured. In contrast to the ANS spin-coating film with poor luninescence polarization (r = 0.07), $(ANS/LDH)_{20}$ UTF displays well-defined luninescence polarization (r = 0.20, Figure 3), indicating an improvement in the overall orientation of the ANS ions between the LDH nanosheets. It can be speculated that the host-guest interaction induced the ANS ions to be arranged into an oriented manner, which may be responsible for the enhanced polarized photoemission.

3 Reversible fluorescence response of the $(ANS/LDH)_n$ UTFs for different polarity environment

The $(ANS/LDH)_n$ UTFs exhibit very weak fluorescence with a broad emission peak at about 468 nm in the dry air or water (Figure S5), which is similar to the ANS-intercalated MgAl-LDH powders[10], and had obviously blue shift compared with that of the ANS-water solution (Figure 4C). Howerever, it displayed different and enhanced fluorescence for different polarity solvents.

Figure 4A shows the fluorescence spectra of $(ANS/LDH)_{10}$ UTF in petroleum ether, toluene, isopropanol, dimethyl formamide and pure water, the fluorescence intensity of $(ANS/LDH)_{10}$ UTF decreases with increasing of the solvent polarity, and concomitant with the red shift of the maximum emission. The fluorescence enhancement of $(ANS/LDH)_{10}$ UTF in low polar solution could be attributed to the changes of intramolecular conformation of the ANS in different polarity environment.[9,10] Moreover, when the $(ANS/LDH)_{10}$ UTF was immersed in ethanol/water solution with different ratio, its fluorescence intensity increased with increasing of the ethanol/water ratio (Figure S6), which further evidenced that. The red shift of the maximum emission peak is due to the various aggregation states in different polar solvent. In addition, the $(ANS/LDH)_{10}$ UTF showed reversible fluorescence changes in different polar solvent, for example, after ten cycles by alternatively treatment with petroteum ether and pure water, the UTF still keep well fluorescence properties (Figure 4B), confirming the stability and reversiblity of the $(ANS/LDH)_n$ UTF for the polarity response, which indicates that this film can be a novel potential fluorescence sensor for the environment polarity.

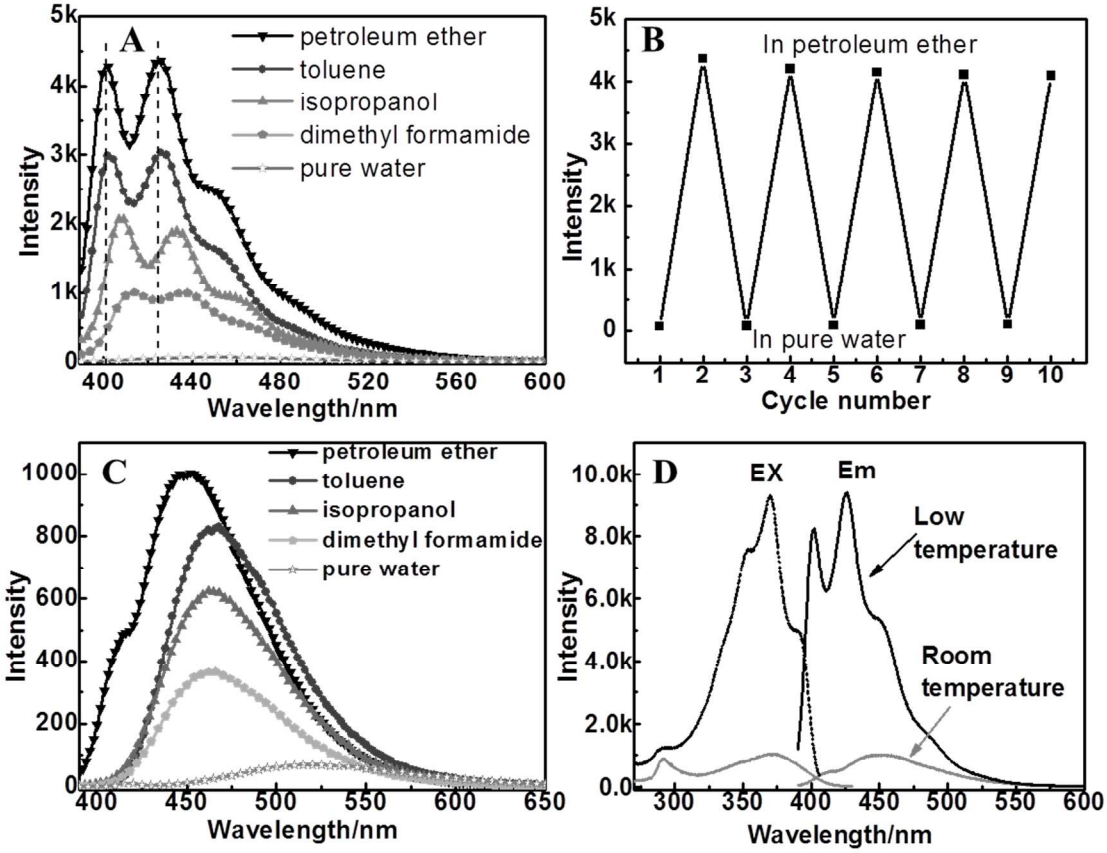

Figure 4.A) Fluorescence spectra of $(ANS/LDH)_{20}$ UTF in different solvents, B) Fluorescence intensityat 425 nm of $(ANS/LDH)_{20}$ UTF subjected to the alternative immersion treatment in pure water and petroleum ether, respectively. C) Fluorescence spectra of ANS in different solvents, D) Fluorescence excitation and emission spectra of ANS in petroleum ether (1μg/mL) at low temperature (-16℃) and room temperature (about 23℃).

To further understand the fluorescence response of the ANS-containing UTFs for different polarity environment, the sensing properties of ANS spin-coating film was tested, but it was found that the single ANS spin-coating film, compared with the $(ANS/LDH)_n$ assembly film, was instable and easy fall off in the tested environment. Experimentally, the spin-coating film showed no obvious changes on the fluorescence peak position and fluorescent shape in different solvent environment, but the tested environment showed fluorescence to some extent due to the

shedding of ANS on the spin-coating film, so it was difficult to test the sensing properties of the ANS spin-coating film, which was not suitable to be used as a fluorescent sensor. However, compared with the fluorescence spectra of ANS solution with different solvents (Figure 4C) which has only one broad peak, the $(ANS/LDH)_n$ UTF in different polar environment show three distinctively different emission peaks. To investigate this difference， the fluorescence properties of ANS/petroleum ether solution were studied (Figure 4D). It was observed that ANS/petroleum ether solution (1μg/mL) showed one broad peak at room temperature, however, it split into three narrow fluorescence peaks at lower temperature (-16℃), similar to the room temperature fluorescence spectra of the $(ANS/LDH)_n$ UTF in different polar environment. Therefore, it can be speculated that LDH laminate provide a 2D restricted space to limit the ANS molecular rotation for the $(ANS/LDH)_n$ UTF, which shows weak fluorescence in dry air or pure water as mentioned earlier, but when the UTF immersed in polar organic solvent, the solvent molecule penetrated into the LDH monolayers and aggreate around the peripherals of the ANS within the interlayers. Its small-angle XRD pattern of the UTF-40 changed after immersion treatment in petroleum ether (Figure 2E), indicated that the thickness of per bilayer augmented from 7.0 nm in dry air to 9.7 nm after treatment with petroleum ether, which can be ascribed to the solvent molcule entered into and swollen the interlayer space of the UTF. This new flourescence properties of the $(ANS/LDH)_n$ UTFs is different with the ANS-intercalated LDH powders,[12,13] which further prove the 2D confinement effect of the LDH laminate for limiting the guest molecules structure in our privous works.[34, 40]

4 Selective fluorescence response of the $(ANS/LDH)_n$ UTFs for various biomolecules

Traditionally, ANS molecule was a non-polar probe for protein. Binding of ANS to ptotein like BSA (Albumin from Bovine Serum) and consequent changes in ANS fluorescence have been studied in detail by many groups.[48-52] The interactions between ANS and BSA were mainly attribute to hydrophobic effect, hydrogen-bond and electrostatic interaction. Hydrophobic interactions occur at sites on BSA in domains II and III,[49-52] electrostatic interaction form between the ANS sulfonate group and the protein cationic side chains,[50,51] hydrogen bond was observed between the sulfonate group of ANS molecule docked at the cavity and H241 of BSA,[52] these bind interactions produced some structural/conformational changes in the surrounding environment and resulted the fluorescence enhancement of ANS. The luminescence properties of the $(ANS/LDH)_n$ UTFs also imply the feasibility as a sensitive fluorescence probe toward the protein. Taking the $(ANS/LDH)_{10}$ UTF as an example, the film exhibit a significant fluorescence enhancement upon increasing the concentration of BSAprotein. Figure 5A shows the fluorescence emission of UTF after immersed into BSA solution with different concentration, while it is not a simple linear relationship betweenthe fluorescence intensity and the BSA concentration (Figure 5B). Under low BSA concentration (0.02 − 0.12 mg/mL) (Figure 5C), the fluorescence intensity of ANS increased slowly with a linear regression equation:

$$I = -13.28 + 2177.78C \text{ (mg/mL)}, r^2 = 0.998. \qquad (1)$$

The detection limit based on IUPAC ($C_{DL} = 3S_b\ m^{-1}$) was 1.37 μg/mL (about 0.02 μM), which is comparable to the reported BSA probes[53-55]. While in high BSA concentration (0.12 − 0.28 mg/mL) the fluorescence intensity increased observably with another linear relationship.

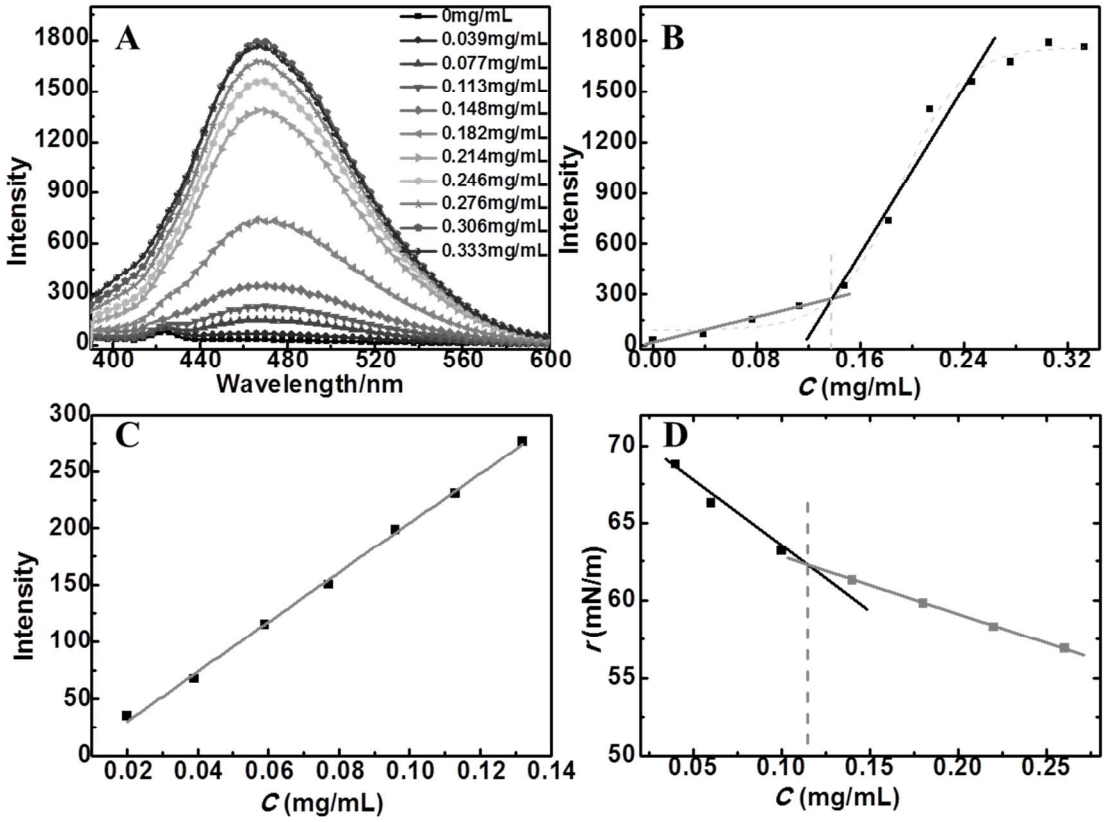

Figure 5. A) Fluorescence spectra of the $(ANS/LDH)_{10}$ UTF after immersion into BSA protein solutions with different concentration (λ_{ex} = 370 nm), B) and C) Plots of fluorescence intensity at 470 nm versus the corresponding BSA concentration, D) Plots of surface tension versus the concentration of BSA.

Through the study of surface tension (γ) of BSA solution with different concentration (Figure 5D), it was found that at low concentration, the BSA were preferentially absorbed at the air-water interface, thus leading to a reduction in the surface tension of water. When the BSA concentration continued to increase, the surface tension of BSA at the air-water interface reduce more slowly, and the inflection point appears at around 0.12mg/mL (1.8 μM), indicative of another aggragation state of BSA. Moreover, the SEM images of BSA prepared by different concentrations (0.04 - 0.22 mg/mL) also showed a intuitive performance of the aggregation

states of the BSA (Figure S8), it showed a obviously different aggregation states at the high concentration (above 0.14 mg/mL). Thus it can explain that the fluorescence intensity increased linearly with the BSA concentration in the range from 0 to 0.12mg/mL, and after which it has another linear relationship. This also indicated that the $(ANS/LDH)_n$ UTFs are more sensitive to the formation of different BSA aggregate state, which means that this kind of UTFs can not only detect the concentration but also monitor the aggregation states of the BSA-like protein.

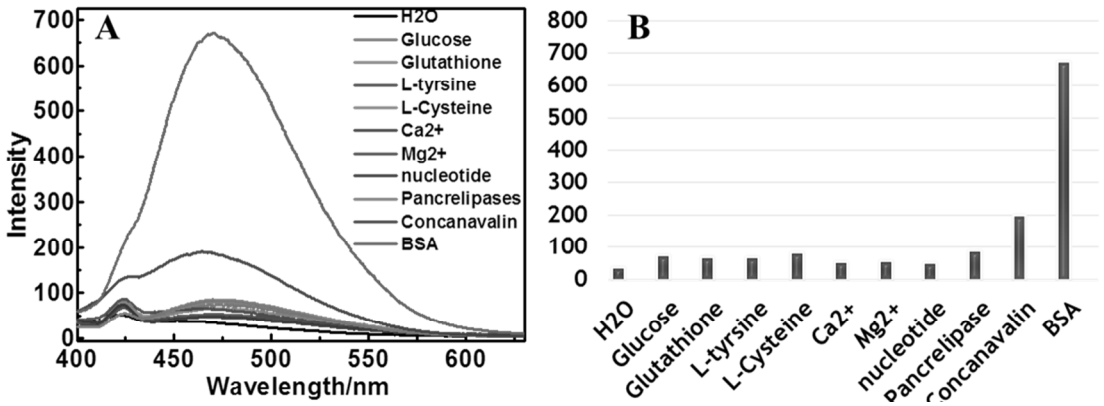

Figure 6.A) Fluorescence spectra and B) fluorescence intensity comparison of $(ANS/LDH)_{10}$ UTF upon addition of glucose, glutathione, L-tyrsine, L-cysteine, Ca^{2+}, Mg^{2+}, nucleotide, pancrelipase, concanavalin and BSA, respectively. All the concentration of these solution are 0.2mg/mL.

Glucose, peptide, amino acid, nucleotide and some small ions are all important biomolecules *in vivo*, it is significant to know how these biomolecules interfere the response of $(ANS/LDH)_{10}$ UTF toward BSA protein. Figure 6 shows the changes of $(ANS/LDH)_{10}$ UTF toward various biomolecules (glucose, glutathione, L-tyrsine, L-cysteine, Ca^{2+}, Mg^{2+}, nucleotide, pancrelipase, concanavalin and BSA), respectively. Only in concanavalin or BSA protein solution, the flourescence intensity of $(ANS/LDH)_n$ UTF is enhanced prominently, and the other biomolecules

has no effect on the flourescence properties of the UTF. Compared with BSA,[56] pancrelipase[57] and concanavalin[58-60] are two kinds proteins with different structure, they have less hydrophobic sites, thus there were not obvious fluorescence enhancement on $(ANS/LDH)_n$ UTF. The results demostrate that the $(ANS/LDH)_n$ UTF can be used as a fluorescence sensor for selective detection of BSA-like protein oreven diferent hydrophobic proteins over range of other biomolecules.

Conclusions

In summary, the small anion ANS was successfully assembled with LDH nanosheets to form $(ANS/LDH)_n$ UTFs by LbL assembly technique. The drive force of the $(ANS/LDH)_n$ system was discussed and attributed to electrostatic interaction and two possible weak interactions−hydrogen bond and induced electrostatic interaction between ANS and positive-charged LDH nanosheets. It was found that the obtained $(ANS/LDH)_n$ UTFs show uniform and long-range-ordered periodic layered structure. This UTFs can sensor fluorescence response of different polarity environment reversibly, and the original broad fluorescence peak split into three induced by the 2D confinement effect of the LDH monolayers and the change of the polar environment, its fluorescence intensity decreases with increasing of the solvent polarity, and concomitant with red shift of the maximum emission peak. Meanwhile, the composite UTFs exhibit selective fluorescence enhancement in the prescence of hydrophobic BSA-like protein biomolecules and the rate of fluorescence enhancement with the concentration is significantly different with the different BSA aggregation state, which may be used not only to detect the protein concentration but also to monitor the aggregation states of the BSA-like protein. Therefore, the $(ANS/LDH)_n$ UTFs is potential to be a novel type of biological flourescence sensor material.

ASSOCIATED CONTENT

Supporting Information

XRD pattern and SEM image of Mg_2Al-NO_3 LDH powders. UV-vis absorption spectra of the ANS solution. The top-view SEM images and side-view SEM images of the $(ANS/LDH)_n$ (n = 8 − 20) UTFs. The AFM images of the $(ANS/LDH)_n$ (n = 8 − 20) UTFs (scanning area is random for 5μm × 5μm). The roughness of the $(ANS/LDH)_n$ (n = 4 − 20). Fluorescence spectra of $(ANS/LDH)_{20}$ UTF inethanol/water solution with different ratio and plots of fluorescence intensity at 464 nm versus the corresponding ethanol/water ratio. ATR-FTIR spectra of LDH-NO_3 and $(ANS/LDH)_{50}$ UTF. SEM images of BSA prepared by different concentration.

AUTHOR INFORMATION

Corresponding Author

*E-mail: lujun@mail.buct.edu.cn. Tel:+86-10-64442146.

Notes

The authors declare no competing financial interest.

ACKNOWLEDGMENT

This work was supported by the 973 Program (grant no.2014CB932101), the National Natural Science Foundation of China, 111 Project (grant no. B07004) and Central University Research funds of China (buctrc201527).

REFERENCES

(1) Morris, M. C.; Blondel, M. Editorial: Fluorescent biosensors. *Biotechnol. J.***2014**, 9, 171-

173.

(2) Ueno, T.; Nagano, T. Fluorescent probes for sensing and imaging. *Nat. Methods.* **2011**, 8, 642-645.

(3) Lavis, L. D.; Raines, R. T. Bright ideas for chemical biology. *ACS Chem. Biol.* **2008**, 3, 142-155.

(4) Rajalingam, D.; Graziani, I.; Prudovsky, I.; Yu, C.; Kumar, T. K. S. Relevance of partially structured states in the non-classical secretion of acidic fibroblast growth factor. *Biochemistry.* **2007**, 46, 9225-9238.

(5) Ma, Z. W.; Piszczek, G.; Wingfield, P. T.; Sergeev, Y. V.; Hejtmancik, J. F. The G18V CRYGS mutation associated with human cataracts increases S-crystallin sensitivity to thermal and chemical stress. *Biochemistry.* **2009**, 48, 7334-7341.

(6) Tagore, R.; Thomas, H. R.; Homan, E. A.; Munawar, A.; Saghatelian, A. A global metabolite profiling approach to identify protein-metabolite interactions. *J. Am. Chem. Soc.* **2008**, 130, 14111-14113.

(7) Ohashi, T.; Augustus, A. M.; Erickson, H. P. Transient opening of fibronectin type III(FNIII) domains: the interaction of the third FNIII domain of FN with anastellin. *Biochemistry.* **2009**, 48, 4189-4197.

(8) Tan, A. M.; Henzl, M. T. Evidence for a Ca^{2+}-specific conformational change in avian thymic hormone, a high-affinity β-parvalbumin. *Biochemistry.* **2009**, 48, 3936-3945.

(9) Kosower, E. M.; Kanety, H. Intramolecular Donor-Acceptor Systems.10. Multiple Fluorescences from 8-(Phenylamino) 1-Naphthalenesulfonates. *J. Am. Chem. Soc.* **1983**, 105, 6236-6243.

(10) Weber, G.; Laurence, D. J. R. Fluorescent Indicators of Adsorption in Aqueous Solution and

on the Solid Phase. *Biochim. J.* **1954**, 56, xxxi.

(11) Buschmann, H. J.; Wolff, T. Fluorescence of 1-anilinonaphthalene-8-sulfonate in solidmacrocyclic environments. *J. Photochem. Photobiol. A: Chem.* **1999**, 121, 99-103.

(12) Sun, Z. Y.; Jin, L.; Shi, W. Y.; Wei, M.; Duan, X. Preparation of an anion dye intercalated into layered double hydroxides and its controllable luminescence properties. *Chem. Eng. J.* **2010**, 161, 293-300.

(13) Sun, Z. Y.; Jin, L.; Shi, W. Y.; Wei, M.; Duan, X. Controllable Photoluminescence Properties of an Anion-Dye-Intercalated Layered Double Hydroxide by Adjusting the Confined Environment. *Langmuir*. **2011**, 27, 7113-7120.

(14) Wang, C. Y.; Ye, S. Q.; Dai, L.; Liu, X. X.; Tong, Z. Enhanced Resistance of Polyelectrolyte Multilayer Microcapsules to Pepsin Erosion and Release Properties of Encapsulated Indomethacin. *Biomacromolecules.* **2007**, 8, 1739-1744.

(15) Tang, T. J.; Qu, J. Q.; Mulllen, K.; Webber, S. E. Molecular Layer-by-Layer Self-Assembly of Water-Soluble Perylene Diimides through π-π and Electrostatic Interactions. *Langmuir* .**2006**, 22, 26–28.

(16) Liang, Z.; Dzienis, K. L.; Xu, J.; Wang, Q. Covalent Layer-by-Layer Assembly of Conjugated Polymers and CdSe Nanoparticles: Multilayer Structure and Photovoltaic Properties. *Adv. Funct. Mater.* **2006**, 16, 542-548.

(17) Zhang, Y. J.; Yang, S. G.; Guan, Y.; Cao W. X.; Xu, J. Fabrication of Stable Hollow Capsules by Covalent Layer-by-Layer Self-Assembly. *Macromolecules.* **2003**, 36, 4238–4240.

(18) Such, G. K.; Johnston, A. P.; Caruso, F. Engineered hydrogen bonded polymer multilayers: from assembly to biomedical applications. *Chem. Soc. Rev.* **2011**, 40, 19-29.

(19) Liang, Z. Q.; Cabarcos, O. M.; Allara, D. L.; Wang, Q. Hydrogen-Bonding-Directed Layer-by-Layer Assembly on Conjugated Polymers. *Adv. Mater*. **2004**, 16, 823–827.

(20) Johnston, A.; Read, E.; Caruso, F. DNA multilayer films on planar and colloidal supports: sequential assembly of like-charged polyelectrolytes. *Nano Lett.* **2005**, 5, 953-956.

(21) Johnston, A. P.; Caruso, F. Stabilization of DNA multilayer films through oligonucleotide crosslinking. *Small.***2008**, 4, 612−618.

(22) Inoue, H.; Sato, K.; Anzai, J. Disintegration of layer-by-layer assemblies composed of 2-iminobiotin-labeled poly(ethyleneimine) and avidin. *Biomacromolecules*. **2005**, 6, 27-29.

(23) Guan, W. J.; Zhou, W. J.; Lu, J.; Lu, C. Luminescent films for chemo- and biosensing. *Chem. Soc. Rev.* **2015**, 44, 6981-7009.

(24) Li, Y.; Wang, X.; Sun, J. Q. Layer-by-layer assembly for rapid fabrication of thick polymeric films. *Chem. Soc. Rev.* **2012**, 41, 5998-6009.

(25) Yan, D. P.; Lu, J.; Wei, M.; Evans, D. G.; Duan, X. Recent advances in photofunctional guest/layered double hydroxide host composite systems and their applications: experimental and theoretical perspectives. *J. Mater. Chem.* **2011**, 21, 13128-13139.

(26) Wang, Q.; O'Hare, D. Recent advances in the synthesis and application of layered double hydroxide (LDH) nanosheets. *Chem. Rev.* **2012**, 12, 4124-4155.

(27) Corma, A.; Fornes, V.; Rey, F.; Cervilla, A.; Llopis, E.; Ribera, A. Catalytic air oxidation of thiols mediated at a $Mo(VI)O_2$ complex center intercalated in a Zn(II)–Al(III) layered double hydroxide host. *J. Catal.* **1995**, 152, 237-242.

(28) Yu, X.; Chang, Z.; Sun, X. M.; Lei, X. D.; Evans, D. G.; Xu, S. L.; Zhang, F. Z. Co-production of high quality NH_4SCN and sulfur slow release agent from industrial effluent using calcined MgAl-hydrotalcite. *Chem. Eng. J.* **2011**, 169, 151-156.

(29) Kameda, T.; Yamazaki, T.; Yoshioka, T. Selective uptake of aromatic compounds from aqueous solutions by Mg–Al layered double hydroxide intercalated with 2,7-naphthalenedisulfonate. *Chem. Lett.* **2009**, 38, 522–523.

(30) Kameda, T.; Tsuchiya, Y.; Yamazaki, T.; Yoshioka, T. Preparation of Mg–Al layered double hydroxides intercalated with alkyl sulfates and investigation of their capacity to take up N,N-dimethylaniline from aqueous solutions. *Solid State Sci.* **2009**, 11, 2060-2064.

(31) Choy, J. H.; Jung, J. S.; Oh, J. M.; Park, M.; Jeong, J.; Kang, Y. K.; Han, O. J. Layered double hydroxide as an efficient drug reservoir for folate derivatives. *Biomaterials.* **2004**, 25, 3059-3064.

(32) Adachi-Pagano, M.; Forano, C.; Besse, J-P. Delamination of layered double hydroxides by use of surfactants. *Chem. Commun.* **2000**, 1, 91-92.

(33) Hibino, T.; Kobayashi, M. Delamination of layered double hydroxides in water. *J. Mater. Chem.* **2005**, 15, 653-656.

(34) Yan, D. P.; Lu, J.; Wei, M.; Han, J. B.; Ma, J.; Li, F.; Evans, D. G.; Duan, X. Ordered poly(p-phenylene)/layered double hydroxide ultrathin films with blue luminescence by layer-by-layer assembly. *Angew. Chem. Int. Ed.* **2009**, 48, 3073-3076.

(35) Yan, D. P.; Lu, J.; Wei, M.; Qin, S. H.; Chen, L.; Zhang, S. T.; Evans, D. G.; Duan, X. Heterogeneous Transparent Ultrathin Films with Tunable-Color Luminescence Based on the Assembly of Photoactive Organic Molecules and Layered Double Hydroxides. *Adv. Funct. Mater.* **2011**, 21, 2497-2505.

(36) Li, S. D.; Lu, J.; Ma, H. K.; Xu, J.; Yan, D. P.; Wei, M.; Evans, D. G.; Duan, X. Ordered blue luminescent ultrathin films by the effective coassembly of tris(8-hydroxyquinolate-5-

sulfonate) aluminum and polyanions with layered double hydroxides. *Langmuir.* **2011**, 27, 11501-11507.

(37) Yan, D. P.; Lu, J.; Chen, L.; Qin, S. H.; Ma, J.; Wei, M.; Evans, D. G.; Duan, X. A strategy to the ordered assembly of functional small cations with layered double hydroxides for luminescent ultra-thin films. *Chem. Commun.* **2010**, 46, 5912-5914.

(38) Li, S. D.; Lu, J.; Ma, H. K.; Yan, D. P.; Li, Z.; Qin, S. H.; Evans, D. G.; Duan, X. Luminous ultrathin films by the ordered micellar assembly of neutral bis(8-hydroxyquinolate) zinc with layered double hydroxides. *J. Phys. Chem. C.* **2012**, 116, 12836-12843.

(39) Qin, Y. M.; Zhang, P.; Lai, L. C.; Tian, Z. Y.; Zheng, S. F.; Lu, J. Luminous composite ultrathin films of the DCM dye assembled with layered double hydroxides and its fluorescence solvatochromism properties for polarity sensors. *J. Mater. Chem. C.* **2015**, 3, 5246-5252.

(40) Han, J. B.; Dou, Y. B.; Yan, D. P.; Ma, J.; Wei, M.; Evans, D. G.; Duan, X. Biomimetic design and assembly of organic composite films with simultraneously enhanced strength and toughness. *Chem. Commun.* **2011**, 47, 5274-5276.

(41) Li, Z.; Lu, J.; Li, S. D.; Qin, S. H.; Qin, Y. M. Orderly ultrathin films based on perylene/poly(N-vinyl carbazole) assembled with layered double hydroxide nanosheets: 2D fluorescence resonance energy transfer and reversible fluorescence response for volatile organic compounds. *Adv. Mater.* **2012**, 24, 6053-6057.

(42) Li, Z.; Lu, J.; Qin, Y. M.; Li, S. D.; Qin, S. H. Two dimensional restriction-induced luminescence of tetraphenyl ethylene within the layered double hydroxide ultrathin films and its fluorescence resonance energy transfer. *J. Mater. Chem. C.* **2013**, 1, 5944-5952.

(43) Shi, W. Y.; Jia, Y. K.; Xu, S. M.; Li, Z. X.; Fu, Y.; Wei, M.; Shi, S. X. A chiroptical switch based on DNA/layered double hydroxide ultrathin films. *Langmuir.* **2014**, 30, 12916-12922.

(44) Kong, X. G.; Rao, X. Y.; Han, J. B.; Wei, M.; Duan, X. Layer-by-layer assembly of bi-protein/layered double hydroxide ultrathin film and its electrocatalytic behavior for catechol. *Biosens. Bioelectron.* **2010**, 26, 549-554.

(45) Zhao, Y.; Li, F.; Zhang, R.; Evans, D. G.; Duan, X. Preparation of Layered Double-Hydroxide Nanomaterials with a Uniform Crystallite Size Using a NewMethod Involving Separate Nucleation and Aging Steps. *Chem. Mater.* **2002**, 14, 4286-4291.

(46) Yan, D. P.; Qin, S. H.; Chen, L.; Lu, J.; Ma, J.; Wei, M.; Evans, D. G.; Duan, X. Thin film of Sulfonated Zinc Phthalocyanine/Layered Double Hydroxide for Achieving Multiple Quantum Well Structure. *Chem. Commun.* **2010**, 46, 8654-8656.

(47) Yan, D. P.; Lu, J.; Ma, J.; Wei, M.; Evans, D. G.; Duan, X. Layer-by-Layer Assembly of Ruthenium(II)Complex Anion/Layered Double Hydroxide Ordered Ultrathin Films with Polarized Luminescence. *Chem. Commun.* **2009**, 6358-6360.

(48) Layton, D.; Symmons, Peter. The effect of some uncoupling agents, ionophorous agents and inhibitors on the fluorescence of ANS bound to bovine serum albumin. *FEBS Letters*. **1973**, 30, 325-328.

(49) Sahu, K.; Mondal, S. K.; Ghosh, S.; Roy, D.; Bhattacharyya, Kankan. Temperature dependence of solvation dynamics and anisotropy decay in a protein: ANS in bovine serum albumin. *J. Chem. Phys.* **2006**, 124, 124909-1-7.

(50) Haskard, C. A.; Li-Chan, E. C. Y. Hydrophobicity of Bovine Serum Albumin and Ovalbumin Determined Using Uncharged (PRODAN) and Anionic (ANS^-) Fluorescent Probes. *J. Agric. Food Chem.* **1998**, 46, 2671-2677.

(51) Celej, M. S.; Dassie, S. A.; Freire, E.; Bianconi, M. L.; Fidelio, G. D. Ligand-induced thermostability in proteins: Thermodynamic analysis of ANS–albumin interaction. *Biochimica et Biophysica Acta.***2005**, 1750, 122-133.

(52) Cattoni, D. I.; Kaufman, S. B.; Flecha. F. L. G. Kinetics and thermodynamics of the interaction of 1-anilino-naphthalene-8-sulfonate with proteins. *Biochimica et Biophysica Acta.***2009,** 1794, 1700-1708.

(53) Peng, L.; Wei, R. R.; Li, K.; Zhou, Z. J.; Song, P. S.; Tong, A. J.A ratiometric fluorescent probe for hydrophobic proteins in aqueous solution based on aggregation-induced emission. *Analyst.* **2013**, 138, 2068-2072.

(54) Suzuki, Y.; Yokoyama, K.A Protein-Responsive Chromophore Based on Squaraine and Its Application to Visual Protein Detection on a Gel for SDS-PAGE. *Angew. Chem.* **2007**, 119, 4175-4177.

(55) Xu, X. J.; Huang, J.; Li, J. J.; Yan, J. W.; Qin, J. G.; Li, Z. A graphene oxide-based AIE biosensor with high selectivity toward bovine serum albumin. *Chem. Commun.* **2011**, 47, 12385-12387.

(56) Sekula, B.; Zielinski, K.; Bujacz, A. Crystallographic studies of the complexes of bovine and equine serum albumin with 3,5-diiodosalicylicacid. *Int. J. Biol.Macromol.* **2013**, 60, 316-324.

(57) Carrière, F.; Withers-Martinez, C.; Tilbeurgh, H.; Roussel, A.; Cambillau, C.; Verger, R. Structure-function relationships of pancreatic lipases. *Fett/Lipid.* **1998**, Nr. 4-5, 96-102.

(58) Zhang, Z.; Qian, M. X.; Huang, Q. C.; Jia, Y. S.; Tang, Y. Q.; Wang, K. Y.; Cui, D. F.; Li, M. Y. Crystal Structure of the Complex of Concanavalin A and Hexapeptide. *J. Protein. Chem.* **2001**, 20, 423-429.

(59) Sean, P.; Bernhard, R.; Hakon, H. Atomic Resolution Structure of Concanavalin At 120 K. *ActaCrvst.* **1996**, D52, 1161-1168.

(60) Karl, D. H.; Clinton, F. A. Structure of Concanavalin A at 2.4-Å Resolution. *Biochemistry.* **1972**, 11, 4910-4919.

TOC Graphic

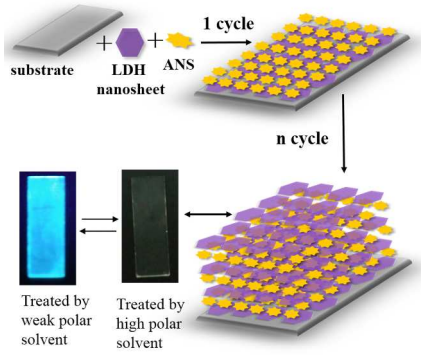

Organic fluorescent dye small anion 8-anilino-1-naphthalenesulfonate (ANS) can assemble with positive-charged layered double hydroxide nanosheets to form ordered $(ANS/LDH)_n$ ultrathin films(UTFs) via the layer-by-layer technique based on electrostatic interaction and weak interactions. This UTFs exhibit reversible fluorescence response of different polar environmentand selective fluorescence response of protein biomolecules, which is potential to be a novel type of fluorescent biosensor materials.